J. Fluid Mech. (1988), *vol.* 191, *pp.* 583–597
Printed in Great Britain

Crossed rolls at onset of convection in a rigid box

By BOYD F. EDWARDS
Department of Physics, West Virginia University, Morgantown, WV 26506, USA

(Received 4 October 1985 and in revised form 4 September 1987)

Critical Rayleigh numbers, roll configurations, and growth-rate derivatives are calculated at onset of convection for a rigid box with conducting upper and lower plates and insulating sidewalls. When the sidewalls form a square or a near square, the linearized Oberbeck–Boussinesq equations favour crossed rolls, a superposition of three-dimensional rolls in the x- and y-directions, over unidirectional rolls. These crossed rolls preserve the four-fold rotation symmetry about the vertical axis of a square box only when the aspect ratio (ratio of width to depth of the box) demands an even number of rolls in each direction. The analysis explains patterns observed by Stork & Müller.

1. Introduction

At a critical temperature gradient, a static fluid layer that is heated from below undergoes a transition to steady convection. In a fluid layer of depth d bounded by rigid horizontal conducting planes, equations linear in the convective amplitude cannot select the physical convective pattern from an infinite number of possibilities, including parallel rolls with axes in any horizontal direction, hexagons, and crossed rolls (Chandrasekhar 1961, chap. II). For this laterally unbounded slab, nonlinear effects must be incorporated in order to identify parallel rolls as the physical convective pattern (Schlüter, Lortz & Busse 1965).

A small aspect ratio box with a rectangular horizontal cross-section restricts the roll axes to two possible horizontal directions prescribed by the sidewalls. For a box with rigid conducting sidewalls, a linear analysis by Davis (1967) showed that 'finite' rolls with two non-zero components of velocity dependent on three spatial coordinates have axes along the short sidewall. Catton (1972*a*) confirmed this result for finite rolls with rigid insulating sidewalls.

In their experiments, Stork & Müller (1972) observed roll axes along the short sidewall when the difference in sidewall lengths was significant. For equal or near-equal sidewall lengths, however, they ascribed their symmetrical convection patterns to combinations of rolls with axes in both horizontal directions. Taking the x- and y-axes normal to the sidewalls and through the centre of the box, rolls with axes perpendicular to the x (y)-axis were termed x-rolls (y-rolls). A single toroidal roll observed for a (horizontally) square box of width $2d$ was viewed as a combination of two x-rolls and two y-rolls. Wider square boxes chose more complicated patterns with less obvious connections to crossed rolls. The calculations by Davis and Catton assuming rolls in only one direction cannot account for these patterns.

Our linear calculations for onset of convection for a rigid box with insulating sidewalls allow combinations of rolls in both horizontal directions. We find that sidewalls require crossed rolls rather than rolls in only one direction and thereby fully remove the degeneracy of the laterally unbounded slab. We emphasize that the

absence of degeneracy at onset of convection for a box allows the physical convective pattern to be chosen by linear theory alone, in contrast to the laterally unbounded slab. Our analysis predicts Stork & Müller's toroidal roll and explains other observed patterns as combinations of perpendicular rolls. When the geometry requires an even number of rolls in each horizontal direction, our crossed rolls resemble the 'cross-roll' instability for a laterally unbounded slab (Clever & Busse 1974). We find, however, that the number of rolls in each direction cannot be determined independently; a square box sometimes requires an odd number of x-rolls and an even number of y-rolls. When the difference in sidewall lengths is large, rolls along the shorter sidewall dominate, consistent with Davis and Catton. Our box widths range between d and $12d$.

Davies-Jones (1970) proved analytically that rigid sidewalls perpendicular to roll spines require three non-zero velocity components. In addition, he calculated the critical Rayleigh number for onset of convection $\mathscr{R}_c$ and the critical wavelength q_c of rolls perpendicular to the sidewalls of a 'channel', a box with one infinite horizontal dimension. Three-dimensional rolls yielded lower $\mathscr{R}_c$ and q_c than finite rolls for free upper and lower plates and rigid sidewalls. Luijkx & Platten (1981) reached the same conclusions for a channel with all-rigid boundary conditions. Accordingly, we find that three-dimensional rolls in a box yield lower $\mathscr{R}_c$ than previous two-dimensional descriptions. Crossed three-dimensional rolls further lower $\mathscr{R}_c$ and often yield fewer rolls (lower q_c) than Davis. Catton's $\mathscr{R}_c$ exceeds our $\mathscr{R}_c$ for crossed rolls by as much as 8% for a square box of width $2d$.

We also calculate the growth-rate derivative σ' at onset of convection for all Prandtl numbers $\mathscr{P}$($\mathscr{P} = \nu/\kappa$, the ratio of kinematic viscosity to thermal diffusivity). In linear Rayleigh–Bénard theory, an infinitesimal-amplitude disturbance about the static state grows (or decays) with time as $e^{\sigma t}$. Near $\mathscr{R}_c$, the growth rate behaves as $\sigma = \sigma'\epsilon$, where $\epsilon = \mathscr{R}/\mathscr{R}_c - 1$ and $\sigma' > 0$. The growth-rate derivative $\sigma' = (d\sigma/d\epsilon)_{\epsilon=0}$ characterizes the divergence of the timescale σ^{-1} at convective onset relevant to 'critical slowing down' (Behringer & Ahlers 1977). Shaumeyer, Behringer & Baierlein (1981) recently reported growth-rate derivatives for a cylinder.

The stability of convective rolls for small-aspect-ratio boxes and small Prandtl numbers relevant to experiments by Maeno, Haucke & Wheatley (1985) and others is currently under investigation.

2. Equations

We write the linearized Oberbeck–Boussinesq equations, which neglect density variations except where they modify gravity (Chandrasekhar 1961, chap. II), in the small perturbations of the velocity $\boldsymbol{V}$, temperature Θ, and pressure P about the static state as

$$\frac{\partial \Theta}{\partial t} = \mathscr{P}^{-1}\nabla^2\Theta + \left(\frac{\mathscr{R}}{\mathscr{P}}\right)^{\frac{1}{2}} W, \tag{1a}$$

$$\frac{\partial \boldsymbol{V}}{\partial t} = \left(\frac{\mathscr{R}}{\mathscr{P}}\right)^{\frac{1}{2}} \Theta\hat{\boldsymbol{z}} + \nabla^2\boldsymbol{V} - \nabla P, \tag{1b}$$

$$\nabla\cdot\boldsymbol{V} = 0. \tag{1c}$$

Here, the Rayleigh number $\mathscr{R} = g\alpha d^3 \Delta T/\kappa\nu$ involves the gravitational acceleration g, the thermal expansion coefficient α, and the excess temperature ΔT of the bottom

plate relative to the top (in conventional units). Length, time, velocity, and temperature are scaled by d, d^2/ν, ν/d and $(\Delta T\nu^2/g\alpha d^3)^{\frac{1}{2}}$.

Like Cross (1980), we conveniently summarize (1a–c) as

$$\frac{\partial \boldsymbol{\Psi}}{\partial t} = \mathbf{L}\boldsymbol{\Psi} - \partial P, \tag{2a}$$

$$\boldsymbol{\nabla} \cdot \boldsymbol{V} = 0, \tag{2b}$$

where $\boldsymbol{\Psi} = (\Theta, \boldsymbol{V}) = (\Theta, U, V, W)$ and $\partial = (0, \boldsymbol{\nabla})$ are column vectors and

$$\mathbf{L} = \begin{pmatrix} \nabla^2/\mathscr{P} & 0 & 0 & (\mathscr{R}/\mathscr{P})^{\frac{1}{2}} \\ 0 & \nabla^2 & 0 & 0 \\ 0 & 0 & \nabla^2 & 0 \\ (\mathscr{R}/\mathscr{P})^{\frac{1}{2}} & 0 & 0 & \nabla^2 \end{pmatrix} \tag{3}$$

is a matrix operator in a temperature–velocity space of four dimensions.

The boundary conditions $\boldsymbol{V} = \Theta = 0$ at $z = \pm\frac{1}{2}$ ensure rigid conducting upper and lower plates. For sidewall lengths l_x and l_y and corresponding aspect ratios $\Gamma_x = l_x/d$ and $\Gamma_y = l_y/d$, the boundary conditions for the rigid insulating sidewalls may be written in rescaled dimensionless coordinates $\xi = x/\Gamma_x$ and $\eta = y/\Gamma_y$. These are $\boldsymbol{V} = \hat{\boldsymbol{n}} \cdot \boldsymbol{\nabla}\Theta = 0$ at $\xi, \eta = \pm\frac{1}{2}$, where $\hat{\boldsymbol{n}}$ is a unit vector normal to the boundary. For these boundary conditions, partial integration reveals the self-adjointness of $\mathbf{L}$ with respect to the inner product $(\boldsymbol{\Psi}_1 \,|\, \boldsymbol{\Psi}_2)$, the volume average of $\boldsymbol{\Psi}_1^{\mathrm{T}} \boldsymbol{\Psi}_2$;

$$(\boldsymbol{\Psi}_1 \,|\, \mathbf{L}\boldsymbol{\Psi}_2) = (\mathbf{L}\boldsymbol{\Psi}_1 \,|\, \boldsymbol{\Psi}_2). \tag{4}$$

3. Variational solution

A variational technique allows us to study the onset of convection. Assuming an exponential time dependence $\boldsymbol{\Psi} \sim \mathrm{e}^{\sigma t}$ and projecting (2a) on to $\boldsymbol{\Psi}$ yields the variational basis

$$\sigma(\boldsymbol{\Psi} \,|\, \boldsymbol{\Psi}) = (\boldsymbol{\Psi} \,|\, \mathbf{L}\boldsymbol{\Psi}), \tag{5}$$

where the pressure term vanishes by partial integration and (2b). We solve (5) by substituting expansions

$$\Theta = \Sigma_{\boldsymbol{m}} C_{\boldsymbol{m}} \Theta_{\boldsymbol{m}}(\boldsymbol{r}), \tag{6a}$$

$$\boldsymbol{V} = \Sigma_{\boldsymbol{m}} [D_{\boldsymbol{m}} \boldsymbol{U}_{\boldsymbol{m}}(\boldsymbol{r}) + E_{\boldsymbol{m}} \boldsymbol{V}_{\boldsymbol{m}}(\boldsymbol{r})], \tag{6b}$$

in functions $\Theta_{\boldsymbol{m}}(\boldsymbol{r})$, $\boldsymbol{U}_{\boldsymbol{m}}(\boldsymbol{r})$ and $\boldsymbol{V}_{\boldsymbol{m}}(\boldsymbol{r})$ whose dependence on the three spatial coordinates is indexed by $\boldsymbol{m} = (m_1, m_2, m_3)$.

The insulating sidewalls allow horizontally uniform modes with $m_1 = 0$ or $m_2 = 0$ in the temperature expansion function,

$$\Theta_{\boldsymbol{m}}(\boldsymbol{r}) = f^{i_1}_{m_1}(\xi) f^{i_2}_{m_2}(\eta)\, \partial_z f^{-i_3}_{m_3}(z), \tag{7a}$$

where the slope of

$$f^i_m(x) = \begin{cases} \delta_{m,0} + (1 - \delta_{m,0})\sqrt{2}\cos 2m\pi x, & i = +1, \\ \sqrt{2}\sin(2m-1)\pi x, & i = -1, \end{cases}$$

vanishes at $x = \pm\frac{1}{2}$. Here, $\delta_{m,n} = 1$ for $m = n$ and vanishes otherwise. Just as $i = +1(-1)$ gives even (odd) $f^i_m(x)$ about $x = 0$, the quantities i_1, i_2 and i_3 give the parity of the temperature in the three spatial directions. These parities are chosen below to produce the desired number of rolls. Equation (1a) ensures that the temperature and vertical velocity have the same parity.

The velocity expansion functions $\boldsymbol{U}_m = (U_m, 0, W_{xm})$ and $\boldsymbol{V}_m = (0, V_m, W_{ym})$ have historical importance. Using expansion functions of the form of $\boldsymbol{U}_m$ (that is, functions with two non-zero components of velocity dependent on three spatial coordinates), Davis (1967) constructed 'finite x-rolls', or two-dimensional rolls with axes perpendicular to the x-axis. For $\Gamma_x > \Gamma_y$, his computations predicted these rolls along the short sidewall rather than 'finite y-rolls' of the form of $\boldsymbol{V}_m$. Davies-Jones (1970) later proved analytically that rigid sidewalls perpendicular to roll spines require three-dimensional rolls. Accordingly, even though $\boldsymbol{U}_m$ dominates for x-rolls, we also include $\boldsymbol{V}_m$ for a complete three-dimensional description of x-rolls. Both expansion functions also describe our y-rolls.

Our explicit velocity expansion functions are identical with those used by Catton (1972*a*) and analogous to those used by Charlson & Sani (1975) for a cylindrical geometry. The vertical components,

$$W_{xm} = \partial_\xi g_{m_1}^{-i_1}(\xi)\, \partial_\eta f_{m_2}^{-i_2}(\eta)\, g_{m_3}^{i_3}(z), \tag{7b}$$

$$W_{ym} = \partial_\xi f_{m_1}^{-i_1}(\xi)\, \partial_\eta g_{m_2}^{-i_2}(\eta)\, g_{m_3}^{i_3}(z), \tag{7c}$$

use complete orthonormal eigenfunctions of ∂_x^4 with vanishing slope and value at $x = \pm\frac{1}{2}$ (Harris & Reid 1958; Chandrasekhar 1961, Appendix V),

$$g_m^i(x) = \begin{cases} C_m(x), & i = +1, \\ S_m(x), & i = -1, \end{cases}$$

and the horizontal components U_m and V_m follow from (2*b*). For economy of notation, the parametric dependence on parity is suppressed on the left-hand sides of (7). The inner products $(\boldsymbol{\Theta}_m | \boldsymbol{\Theta}_m)$, $(\boldsymbol{U}_m | \boldsymbol{U}_m)$ and $(\boldsymbol{V}_m | \boldsymbol{V}_m)$ are normalized to unity by including suitable coefficients on the right-hand sides of (7). Since vanishing components of $\boldsymbol{m}$ have meaning only in uniform temperature modes, we take $D_m = E_m = 0$ for $m_1 = 0$ or $m_2 = 0$.

Our representation in terms of $\boldsymbol{U}_m$ and $\boldsymbol{V}_m$ is general because (1*c*) allows only two independent velocity components. This generality is also evident in an equivalent potential formulation. To satisfy (1*c*), $\boldsymbol{V}$ may always be written as $\boldsymbol{V} = \boldsymbol{\nabla} \times \boldsymbol{A}$. Since an arbitrary gauge transformation $\boldsymbol{A}' = \boldsymbol{A} + \boldsymbol{\nabla}\chi$ cannot change the velocity, we can choose $\partial_z \chi = -\boldsymbol{A} \cdot \hat{\boldsymbol{z}}$. Expanding the components of the resulting $\boldsymbol{A}' = \phi' \hat{\boldsymbol{x}} + \psi' \hat{\boldsymbol{y}}$ in functions

$$\phi'_m = \partial_\xi f_{m_1}^{-i_1}(\xi)\, g_{m_2}^{-i_2}(\eta)\, g_{m_3}^{i_3}(z), \quad \psi'_m = g_{m_1}^{-i_1}(\xi)\, \partial_\eta f_{m_2}^{-i_2}(\eta)\, g_{m_3}^{i_3}(z)$$

yields a representation wholly equivalent to (6*b*). The functions $f_m^i(x)$, $\partial_x f_m^i(x)$ and $g_m^i(x)$ are complete on the interval $-\frac{1}{2} < x < \frac{1}{2}$ for $i = \pm 1$, guaranteeing the full description of general three-dimensional flows. Using gauge transformations, solutions in our representation $\boldsymbol{A}'$ can always be written in other general representations (such as $\boldsymbol{A}'' = \boldsymbol{\nabla} \times \hat{\boldsymbol{z}}\phi'' + \hat{\boldsymbol{z}}\psi''$, Clever & Busse 1974) and vice versa.

With explicit expansion functions, we proceed to solve the variational problem. Substituting the expansions, (6), and varying the coefficients C_m, D_m and E_m reduces (5) to a linear algebraic eigenvalue problem

$$\boldsymbol{A}_{mn} x_n = \sigma \boldsymbol{B}_{mn} x_n \tag{8}$$

with an eigenvector $x_m = (C_m, D_m, E_m)$ and eigenvalue σ. Here, the matrices $\boldsymbol{A}_{mn}$ and $\boldsymbol{B}_{mn}$ are symmetric,

$$\boldsymbol{A}_{mn} = \begin{pmatrix} \mathscr{P}^{-1}(\Theta_m|\nabla^2\Theta_n) & \gamma(\Theta_m|W_{xn}) & \gamma(\Theta_m|W_{yn}) \\ \gamma(W_{xm}|\Theta_n) & (U_m|\nabla^2 U_n) & (U_m|\nabla^2 V_n) \\ \gamma(W_{ym}|\Theta_n) & (V_m|\nabla^2 U_n) & (V_m|\nabla^2 V_n) \end{pmatrix}$$

$$\boldsymbol{B}_{mn} = \begin{pmatrix} (\Theta_m|\Theta_n) & 0 & 0 \\ 0 & (U_m|U_n) & (U_m|V_n) \\ 0 & (V_m|U_n) & (V_m|V_n) \end{pmatrix},$$

$\gamma = (\mathscr{R}/\mathscr{P})^{\frac{1}{2}}$, and sums on $\boldsymbol{n}$ are implied. Recalling that $f^i_m(x)$ and $g^i_m(x)$ are respective eigenfunctions of ∂_x^2 and ∂_x^4 allows us to evaluate the elements of $\boldsymbol{A}_{mn}$ and $\boldsymbol{B}_{mn}$ analytically by partial integration (see also Reid & Harris 1958). The temperature coefficient C_{00m_3} decouples from the equations and is therefore taken to be zero.

Equation (8) separates into eight decoupled eigenvalue problems corresponding to the eight combinations of $i_1 = \pm 1$, $i_2 = \pm 1$ and $i_3 = \pm 1$. The parity combination yielding the lowest critical Rayleigh number is relevant at onset of convection. Because the problem separates, states at onset of convection consequently have definite parity, that is, the temperature and the velocity components are either symmetric or antisymmetric in each coordinate direction. This general property of states at onset of convection arises ultimately from the box boundary conditions, and does not depend on the details of the representation.

The mode indices $\boldsymbol{m}$ retained in x_m deserve attention. We identify the indices retained for x-rolls; indices retained for y-rolls follow by taking $m_1 \rightleftharpoons m_2$ and $i_1 \rightleftharpoons i_2$. The principal index $m_{1\mathrm{p}} = 2^{-1}[N + \frac{1}{2}(1 - i_1)]$ corresponds to an even (odd) number N of x-rolls for $i_1 = +1(-1)$. The neighbouring indices $m_1 = m_{1p} - 1$ and $m_{1p} + 1$ provide corrections to the roll shapes if allowed by the condition $m_1 \geqslant 0$. Even spinal parity $i_2 = +1$ with $m_2 = 0, 1, 2$ ensures conventional rolls, each with uniform sense of rotation, whereas odd spinal parity $i_2 = -1$ with $m_2 = 1, 2$ divides a roll at its spinal midplane ($y = 0$) into half-rolls rotating in opposite directions. Taking $i_3 = +1$ and $m_3 = 1, 2$ gives a single horizontal layer of rolls relevant to aspect ratios of unity or greater. Including the various combinations of m_1, m_2 and m_3 for x-rolls in the eigenvector x_m along with combinations for y-rolls yields eigenvalue problems with less than 100 unknown coefficients. The value of $\mathscr{R}$ yielding $\sigma = 0$ in (8) is the critical Rayleigh number for onset of convection $\mathscr{R}_\mathrm{c}$. Minimizing $\mathscr{R}_\mathrm{c}$ with respect to the number of x-rolls and y-rolls gives the preferred pattern at onset of convection.

A test case with $\Gamma_x = 2$ and $\Gamma_y = 1.4$ indicates the numerical precision of our procedure at small aspect ratios. For two x-rolls (with $m_{1\mathrm{p}} = 1$) described by $m_1 = m_{1\mathrm{p}} - 1, m_{1\mathrm{p}}, \ldots, m_{1\mathrm{p}} + M, m_2 = 0, 1, \ldots, 1 + M$ and $m_3 = 1, \ldots, 1 + M$ and two weaker y-rolls described similarly, the successive approximations $M = 0$, $M = 1$ (used in the computations, see last paragraph of this section), and $M = 2$ yield $\mathscr{R}_\mathrm{c} = 2677$, 2417 and 2390. This and similar convergence of the growth-rate derivative at $\mathscr{P} = 0.066$ (§4), $\sigma' = 41.74$, 42.31 and 42.47, indicate high precision for $M = 1$ in $\mathscr{R}_\mathrm{c}$ and σ' at small aspect ratios. The relative contributions of successive terms in a single computation of $I = (\Psi|\Psi)$ for $M = 2$ provide an additional convergence test. Defining I_M as the contribution to I of terms involving modes defined by M (so that $I_2 \equiv I$), we obtain $|I_1 - I_0|/I_0 = 0.028$ and $|I_2 - I_1|/I_1 = 0.002$ at onset of convection.

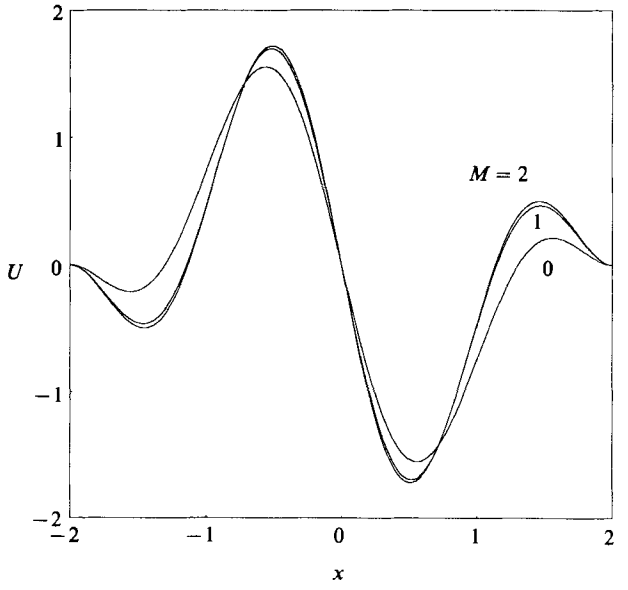

FIGURE 1. Velocity U in the x-direction at onset of convection as a function of x at $y = 0$ and $z = 0.4$, with the origin of coordinates at the centre of a box of horizontal dimensions (relative to the depth) $\Gamma_x = 4$ and $\Gamma_y = 4$. The integers $M = 0, 1$ and 2 label successively better approximations.

Thus, the convergence of our approximate solutions for this box geometry is comparable to the convergence of similar solutions for a laterally unbounded slab (Edwards & Fetter 1984) which agree with exact results.

To demonstrate the precision of our eigenfunctions, we plot the x-component of velocity U as a function of x at $y = 0$, $z = 0.4$ and $\Gamma_x = \Gamma_y = 4$ for the successive approximations $M = 0, 1$ and 2 (labelled by integers on figure 1). The corresponding critical Rayleigh numbers are $\mathscr{R}_c = 1943$, 1827 and 1819. The eigenfunctions are normalized so that $(\Psi|\Psi) = 1$ at each level of approximation. Henceforth, the approximation $M = 1$ is used.

4. Growth-rate derivative

Of interest to experiments is the growth-rate derivative at convective threshold, $\sigma' = (\mathrm{d}\sigma/\mathrm{d}\epsilon)_{\epsilon=0}$. To find its dependence on $\mathscr{P}$, we examine infinitesimal-amplitude perturbations at $\mathscr{R} > \mathscr{R}_c$, where they actually grow with time, using an approach similar to one used by Shaumeyer *et al.* (1981) for a cylinder. Specifically, we evaluate (5) at $\mathscr{R}/\mathscr{R}_c = 1+\epsilon$, $\sigma = \sigma'\epsilon$, $\Psi = \Psi_c + \Psi'\epsilon$, and corresponding $\mathbf{L} = \mathbf{L}_c + \mathbf{L}'\epsilon$ with $\mathrm{L}'_{14} = \mathrm{L}'_{41} = 2^{-1}(\mathscr{R}_c/\mathscr{P})^{\frac{1}{2}}$, otherwise $\mathrm{L}'_{\alpha\beta} = 0$. To first order in ϵ, the self-adjointness of $\mathbf{L}$ and the onset condition $\mathbf{L}_c\,\Psi_c = 0$ reduce (5) to $\sigma' = (\mathscr{R}_c/\mathscr{P})^{\frac{1}{2}}(\Theta_c|W_c)/(\Psi_c|\Psi_c)$. At critical conditions ($\sigma = 0$) in (1), a rescaled critical temperature $\Theta_c^* = \mathscr{P}^{-\frac{1}{2}}\Theta_c$ shares the $\mathscr{P}$-dependence of V_c. Hence, the explicit Prandtl-number dependence of σ' is

$$\sigma'(\mathscr{P}) = \frac{(\mathscr{R}_c)^{\frac{1}{2}}(\Theta_c^*\,|\,W_c)}{\mathscr{P}(\Theta_c^*\,|\,\Theta_c^*) + (V_c\,|\,V_c)}. \tag{9}$$

For convenience, we rewrite $\sigma'(\mathscr{P})$ in terms of $\sigma'(0)$ and $\sigma'(1)$ as

$$\sigma'(\mathscr{P})^{-1} = \sigma'(0)^{-1} + \mathscr{P}[\sigma'(1)^{-1} - \sigma'(0)^{-1}]. \tag{10}$$

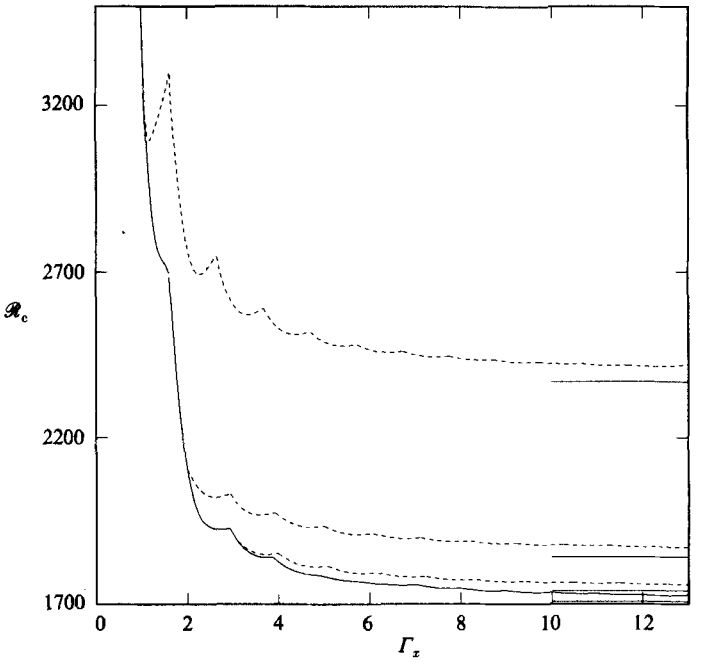

FIGURE 2. Critical Rayleigh number for onset of convection $\mathscr{R}_c$ versus the x-aspect ratio Γ_x. The top, middle, and bottom dashed curves and the solid curve correspond to the y-aspect ratios $\Gamma_y = 1, 2, 3$ and Γ_x respectively. The four horizontal line segments give the corresponding large-Γ_x limits.

According to (9), a single calculation of Ψ_c and $\mathscr{R}_c$ at $\mathscr{P} = 1$ yields

$$\sigma'(0) = (\mathscr{R}_c)^{\frac{1}{2}}(\Theta_c|W_c)/(V_c|V_c), \quad \sigma'(1) = (\mathscr{R}_c)^{\frac{1}{2}}(\Theta_c|W_c)/(\Psi_c|\Psi_c).$$

Equation (10) then supplies the growth-rate derivative at all $\mathscr{P}$. Shaumeyer *et al.* (1981) inferred $\sigma'(1)$ and $\sigma'(\infty)$ relevant to their (18) from numerical computations of σ at $\epsilon \ll 1$ for $\mathscr{P} = 1$ and $\mathscr{P} = \infty$.

5. Results and discussion

To determine the preferred pattern in a square box with $\Gamma_x = \Gamma_y$, we first minimize $\mathscr{R}_c$ in the number N of x-rolls in the absence of y-rolls. Then, with N fixed at the minimum N_c, minimization in the number of superposed y-rolls completes the procedure. We find that an even number N_c of x-rolls requires the same number of y-rolls of equal strength. These reinforce each other at the centre of the box and thereby preserve the four-fold rotation symmetry about the vertical axis. In contrast, odd N_c breaks this symmetry by choosing $N_c - 1$ weaker y-rolls. The corresponding odd spinal parity of these y-rolls requires opposite senses of rotation on either side of their spinal midplane (§4). In general, whatever the value of N_c, the number of y-rolls must be even as long as the x-rolls are symmetric about their spinal midplanes ($i_2 = +1$). Otherwise, the i_2 for the two flows do not agree and the differential equations separate into two uncoupled sets. This requirement of an even number of y-rolls is the key to the remarkable symmetry properties of square boxes at onset of convection.

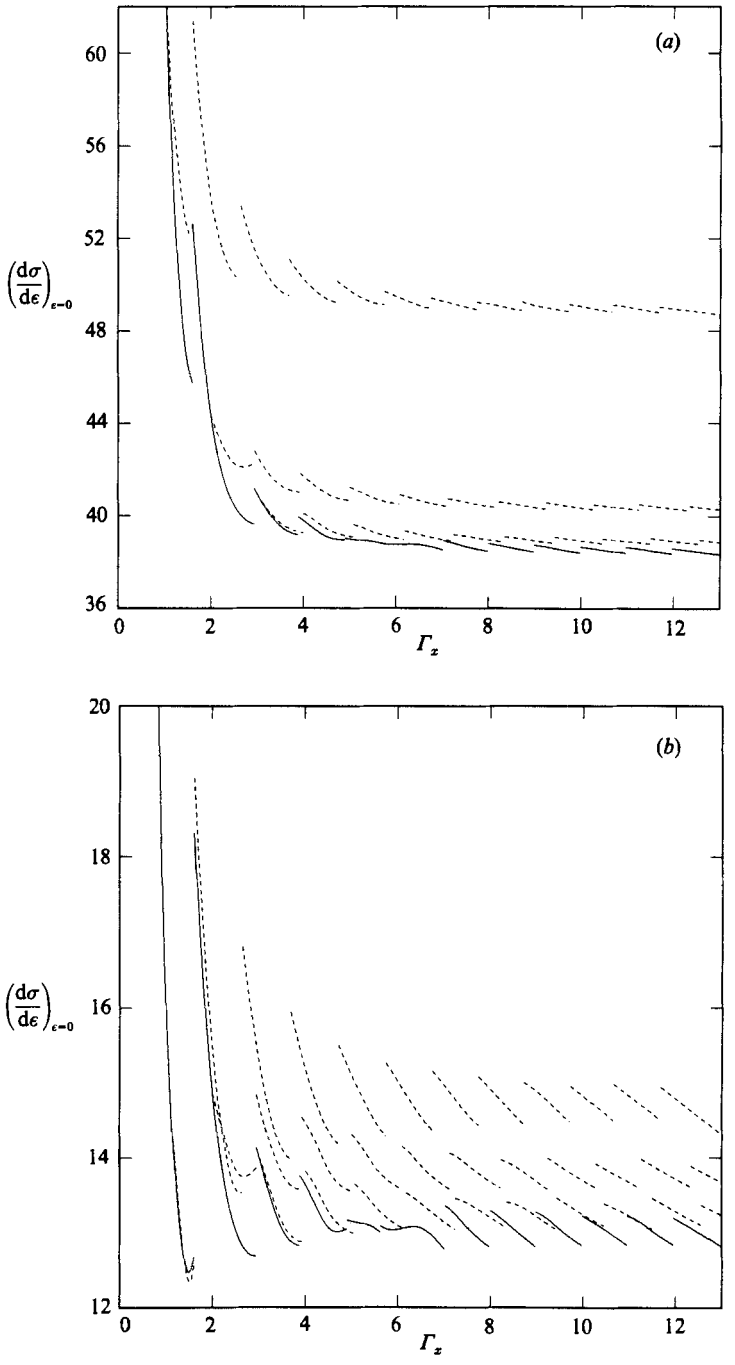

FIGURE 3. Derivative of the growth rate σ with respect to $\epsilon = \mathscr{R}/\mathscr{R}_c - 1$ evaluated at onset of convection $\epsilon = 0$ for Prandtl numbers (*a*) $\mathscr{P} = 0$ and (*b*) $\mathscr{P} = 1$ as a function of the x-aspect ratio Γ_x. The top, middle, and bottom dashed curves and the solid curve are, respectively, for $\Gamma_y = 1$, 2, 3 and Γ_x. The growth-rate derivative $\sigma'(\mathscr{P}) = (d\sigma/d\epsilon)_{\epsilon=0}$ for arbitrary $\mathscr{P}$ follows from (10).

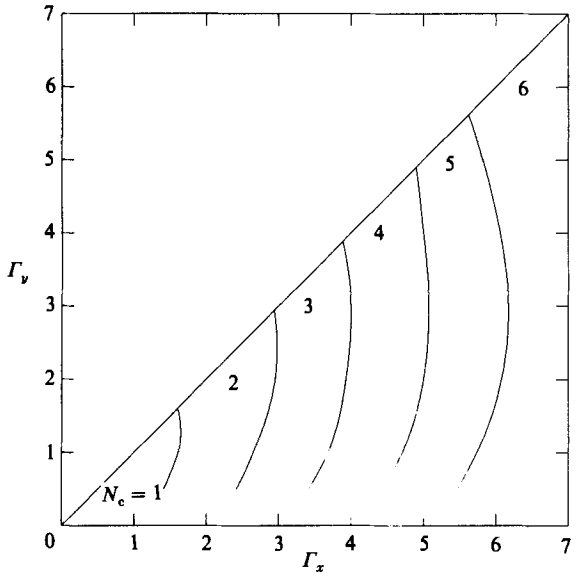

FIGURE 4. Phase diagram of the number of rolls perpendicular to the x-axis (internal numbers) as a function of the box aspect ratios Γ_x and $\Gamma_y < \Gamma_x$, for different N_c.

Calculated values of $\mathscr{R}_c$ show that linear theory favours crossed rolls over parallel rolls in square boxes with small aspect ratios. For $\Gamma_x = \Gamma_y = 2, 6, 12$, we obtain $\mathscr{R}_c = 2219, 1774, 1729$ for x-rolls and $\mathscr{R}_c = 2107, 1765, 1729$ for crossed rolls. Thus, crossed rolls are clearly preferred at small aspect ratios because of their significantly smaller $\mathscr{R}_c$. At large aspect ratios, $\mathscr{R}_c$ converges for the two configurations, reflecting the degeneracy of the laterally unbounded slab. Catton (1972*a*) obtains the corresponding values $\mathscr{R}_c = 2276, 1797, 1741$. His value $\mathscr{R}_c = 2276$ for $\Gamma_x = \Gamma_y = 2$ is near our value for finite x-rolls, $\mathscr{R}_c = 2277$, obtained by neglecting V_m.

Figure 2 shows our calculated $\mathscr{R}_c$ for square boxes (solid trace) as a function of $\Gamma_x = \Gamma_y$. The value $\mathscr{R}_c = 1708$ for a laterally unbounded slab (lowest horizontal line segment) is shown for comparison. Cusps divide regimes of different N_c starting at $N_c = 1$ for $\Gamma_x = 1$; N_c increases by one at each cusp. Values of $\mathscr{R}_c$ were calculated at integral and half-integral values of Γ_x; cubic splines interpolate between the $\mathscr{R}_c$ at given N_c. $\mathscr{R}_c$ for given N_c is shown only to its intersection with neighbouring curves for $N_c - 1$ and $N_c + 1$, even though larger ranges were calculated.

The preferred convective pattern in rectangular geometries satisfying $\Gamma_x > \Gamma_y$ is determined by fixing the number of y-rolls at the value appropriate to a square box of aspect ratio Γ_y and minimizing the Rayleigh number with respect to the number of x-rolls. Figure 2 shows the resulting $\mathscr{R}_c$ for $\Gamma_y = 1, 2, 3$ (top, middle, bottom dashed traces). The data converges with increasing Γ_x to corresponding values obtained by Luijkx & Platten (1981) for an infinite channel (horizontal line segments); our values at $\Gamma_x = 12$ exceed theirs by less than 2%.

Figures 3(*a*) and 3(*b*) shows the growth-rate derivative $\sigma' = (\mathrm{d}\sigma/\mathrm{d}\epsilon)_{\epsilon=0}$ at $\mathscr{P} = 0$ and 1, respectively. As in figure 2, the top, middle, and bottom dashed traces are for fixed $\Gamma_y = 1$, 2 and 3 and the solid trace is for $\Gamma_x = \Gamma_y$. For large Γ_x, the solid traces converge to the values $\sigma'(0) = 38.41$ and $\sigma'(1) = 13.00$ for a laterally unbounded slab (Behringer & Ahlers 1977; Stewartson & Weinstein 1979). Values of $\sigma'(\mathscr{P})$ at arbitrary $\mathscr{P}$ follow by reading values for $\sigma'(0)$ and $\sigma'(1)$ from figures 3(*a*) and 3(*b*) and

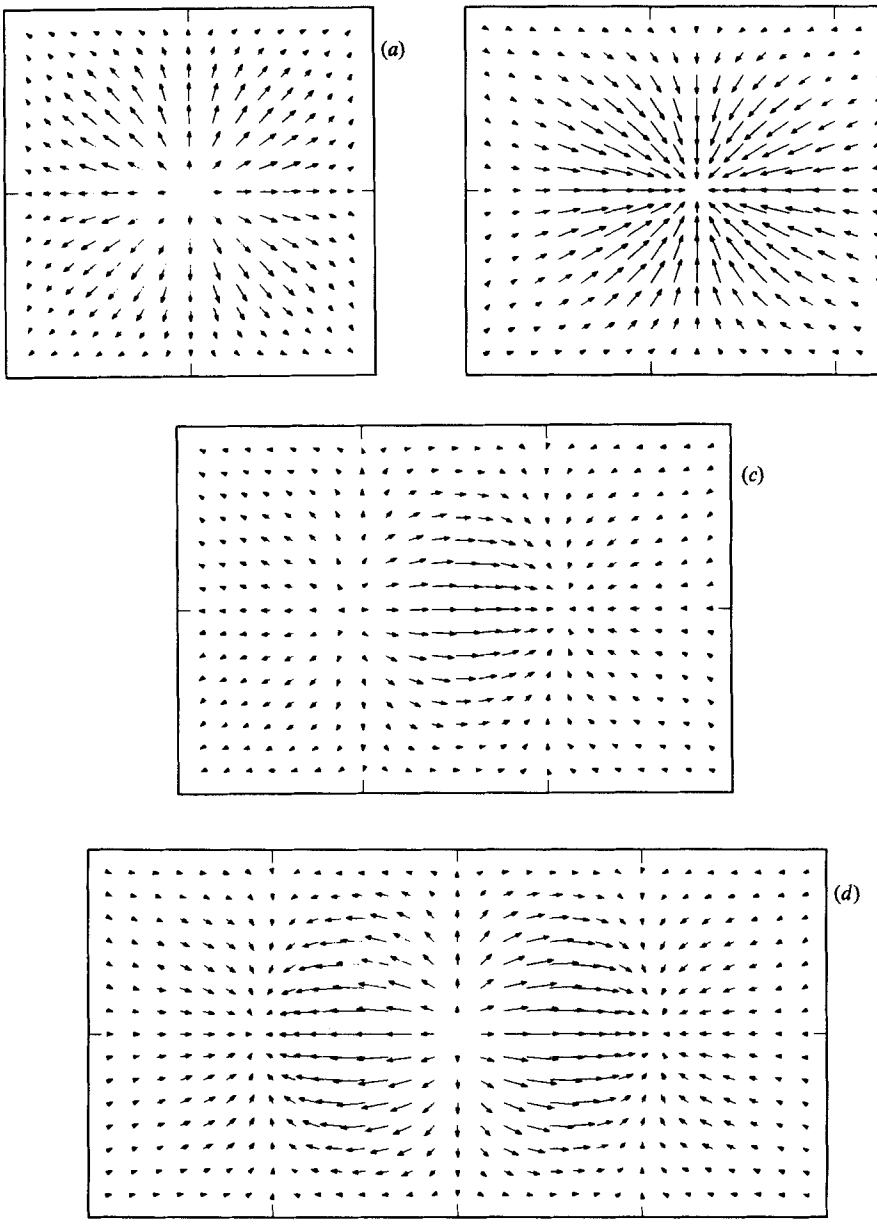

FIGURE 5. Horizontal velocity vectors at onset of convection at $z = 0.4$ for aspect ratios $\Gamma_y = 2$ and (*a*) $\Gamma_x = 2$, (*b*) 2.5, (*c*) 3 and (*d*) 4.

by applying (10). With time $\tilde{t}$ measured in seconds, disturbances about the static conduction state in the velocity or temperature fields near onset grow (or decay) as $\exp[\nu d^{-2}\sigma'(\mathscr{P})\epsilon\tilde{t}]$. Furthermore, the decay rate of small disturbances about steady small-amplitude flows is $2\sigma = 2\sigma'\epsilon$ (Behringer & Ahlers 1977). These relations can be used for direct comparison with experiments.

Unit changes in N_c produce discontinuities in our σ' as a function of Γ_x. In contrast, Shaumeyer *et al.* (1981) report a continuous σ' for concentric rolls in a cylinder. This is to be expected from symmetry considerations. Concentric rolls in a

cylinder have even vertical velocity about reflection of the Cartesian x-axis, $W(-x) = W(x)$, regardless of the number of rolls, whereas rolls in a box may have either parity, $W(-x) = \pm W(x)$. In a box, unit changes in N_c reverse the parity of the solution. Although $\mathscr{R}_c$ is continuous at parity reversals by construction, its derivatives and σ' need not be continuous for a box. For concentric rolls in a cylinder, however, true solutions for $\mathscr{R}_c$, its derivatives, and σ' must be continuous functions of the aspect ratio. In fact, for increasing cylindrical aspect ratio Γ (ratio of radius to depth), Charlson & Sani (1970) reported gradual formation of new rolls (see their figure 8) at the cylinder wall. The apparent cusps in $\mathscr{R}_c$ as a function of Γ in their figure 7 for insulating rigid sidewalls are apparently artifacts of their interpolation procedure; their table 2 indicates a smooth $\mathscr{R}_c$. The cusps in our figure 2 and the discontinuities in our figure 3 are real.

Figure 4 shows the regimes of different N_c (labelled by values of N_c) for small aspect ratios; curves in figure 4 connect the values of (Γ_x, Γ_y) at the cusps in figure 2. Since the $\mathscr{R}_c$ at particular values of N_c become flat functions of Γ_x at large aspect ratios, their intersections (cusps) are sensitive to small changes in $\mathscr{R}_c$. Thus, in the absence of very accurate calculations of $\mathscr{R}_c$, the accuracy of diagrams like figure 4 may suffer at larger aspect ratios. Nevertheless, the agreement with Stork & Müller's measurements is good (see their figure 10). Where figure 4 differs from figure 13 of Davis for conducting sidewalls, it generally predicts one fewer roll.

Koschmieder (1966) observed a 'square' pattern for a square box of aspect ratio $\Gamma = (12.25, 12.25)$ composed of 12 rolls in each horizontal direction (his figure 11). For $\Gamma = (11.43, 11.43)$, however, he obtained a combination of rolls and squares (his figure 13) not describable as simple combinations of x-rolls and y-rolls. Our analysis predicts his square pattern but probably requires a large number of terms to describe his other pattern. The effective degeneracy of parallel rolls and crossed rolls at $\Gamma_x = \Gamma_y = 12$ (see above) indicates that other patterns, possibly including his combination of rolls and squares, might be similarly degenerate at this large aspect ratio. Apparently, as is necessary for the laterally unbounded slab, this large-aspect-ratio box requires a nonlinear analysis to determine the physical convective pattern.

Our linear treatment cannot predict the overall direction of circulation of the flow (if Ψ is a solution, then $-\Psi$ is also a solution), but it does predict the direction of the y-rolls relative to the x-rolls. Horizontal velocity vectors at $z = 0.4$ in figures 5(*a*) and 7(*a*) for the square boxes $\Gamma_x = \Gamma_y = 2$ and 4 show that even values of N_c give equally strong x-rolls and y-rolls that reinforce each other at a central node. Figure 5(*b*) for $\Gamma_x = 2.5$ and $\Gamma_y = 2$ mimics the flow in figure 5(*a*), even though the two x-rolls dominate. For patterns with odd N_c (figures 6*a* and 8), x-rolls and y-rolls reinforce each other at two oppositely directed nodes near the centre of the box, even though the x-rolls clearly dominate.

Improved understanding of the flow fields results from vertical-symmetry considerations. Since $W(-z) = W(z)$ ($i_3 = +1$), (1*c*) requires odd horizontal velocity components about $z = 0$; $\hat{z} \times V(-z) = -\hat{z} \times V(z)$. Therefore, flow fields at $z = -0.4$ follow from those at $z = 0.4$ in figures 5–8 by simply reversing the directions of the horizontal velocity vectors. The resulting flow field in figure 5(*c*) complements figure 17 of Dallmann (1985) showing streamlines near onset of oscillations where, apparently, three rolls are relevant for $\Gamma = (4, 2)$. Interestingly, Dallmann reported no closed three-dimensional streamlines.

Nodes occur where regions of maximum vertical velocities in the x-rolls and y-rolls reinforce each other. In the two-dimensional velocity plots, nodes appear as sources or sinks of velocity. If rolls whose sense of rotation changes at $x = 0$ are handled

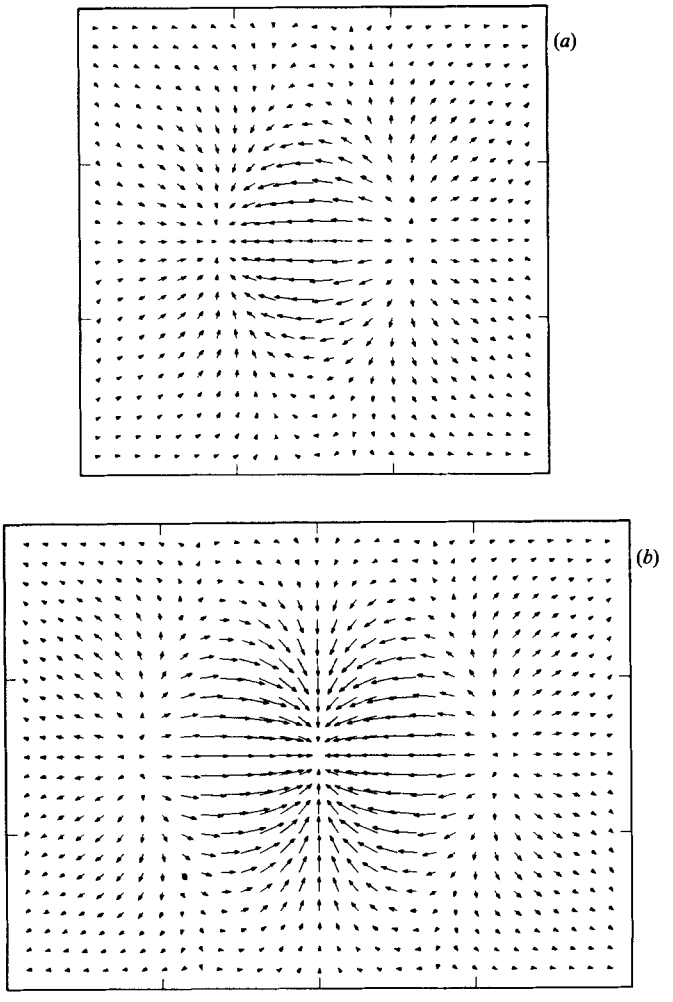

FIGURE 6. Horizontal velocity vectors at $z = 0.4$ for (*a*) $\Gamma_x = 3$ and (*b*) 4, with $\Gamma_y = 3$.

properly, the locations of all the nodes for any specified roll pattern may be estimated by assuming equally spaced rolls in each direction. For example, the nodes at $(x, y) = (\sim \pm\frac{1}{2}, 0)$ and $(\pm\frac{3}{2}, \pm\frac{3}{2})$ in figure 6(*a*) follow from three x-rolls, each with a uniform sense of rotation and width 1, and two y-rolls, each with width 1.5 and changing sense of rotation at $x = 0$, which reinforce each other at $(\frac{1}{2}, 0)$. Opposition at $(\frac{1}{2}, 0)$ would instead yield only boundary nodes at $(x, y) = (\pm\frac{3}{2}, 0)$ and $(\sim \pm\frac{1}{2}, \pm\frac{3}{2})$. In all cases that we considered, the x-rolls and y-rolls reinforced each other near the centre of the box, either as a single node at the centre for even N_c, or as two oppositely directed nodes near the centre for odd N_c. This method may be applied in reverse to extract the orthogonal (or other) roll configurations from the positions of the nodes in a given experimental flow pattern.

Our figures 5–8 display important features of experimental flows observed by Stork & Müller. (In their pictures, regions of large vertical velocity are dark.) Notably, our figures 5(*a*), 7(*a*) for $\Gamma_x = \Gamma_y = 2, 4$ and the corresponding figures 5(*c*), 6(*g*) of Stork & Müller agree that the number of rolls in each direction is Γ_x and that the crossed patterns have comparable amplitudes, thereby preserving the fourfold rotation

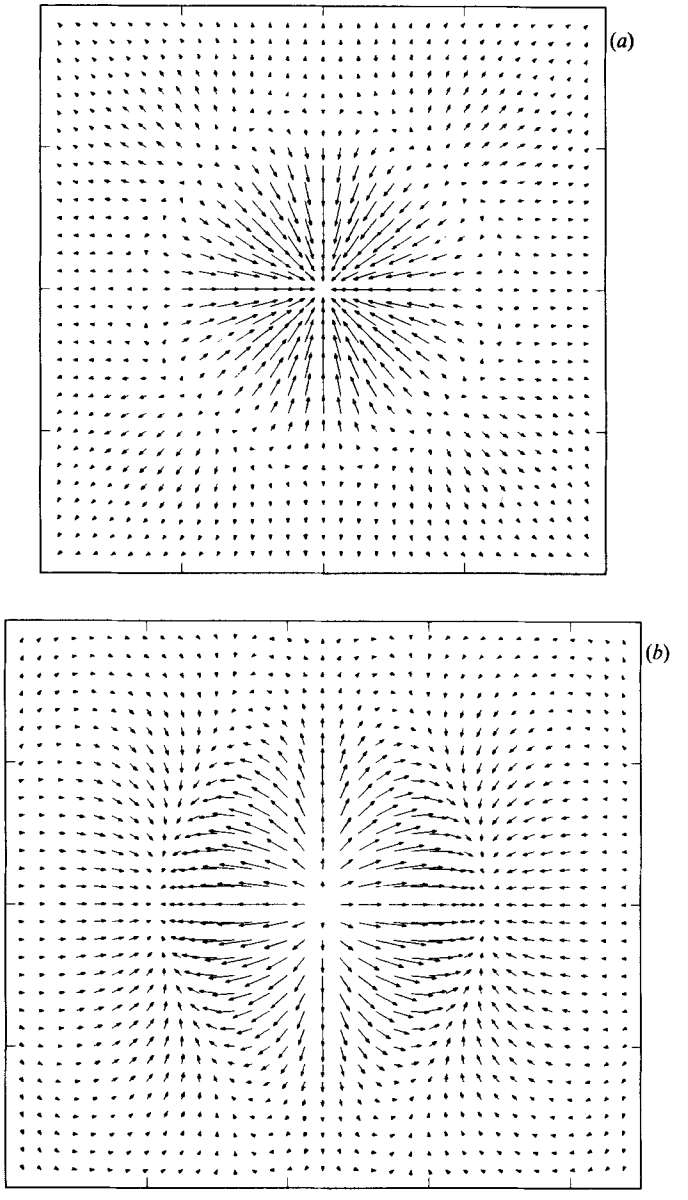

FIGURE 7. Horizontal velocity vectors at $z = 0.4$ for (*a*) $\Gamma_x = 4$ and (*b*) 4.5, with $\Gamma_y = 4$.

symmetry of the box. Figure 5(*a*) is also similar to the single toroidal roll preferred by a cylinder with equal radius and depth (Charlson & Sani 1970). For rectangular boxes, the ends of the outermost rolls observed by Stork & Müller bend toward the box centre (see their figures 5*d–f* and 8*c* for examples). This three-dimensional effect is also evident from our figures 6(*b*) and 7(*b*). Our pattern for $\Gamma = (\Gamma_x, \Gamma_y) = (5, 5)$ (figure 8, $N_c = 5$) corresponds to Stork & Müller's pattern for $\Gamma = (4.5, 4)$ (their figure 9*c*) rather than for $\Gamma = (5.1, 5.0)$ (their figure 7*g*). The shorter sidewall of their figure 9*c* ($\Gamma_y = 4$) partially removes the stagnant regions evident in the upper and lower middle of our figure 8. For $\Gamma = (4.5, 4)$, our calculated $\mathscr{R}_c = 1828$ for their

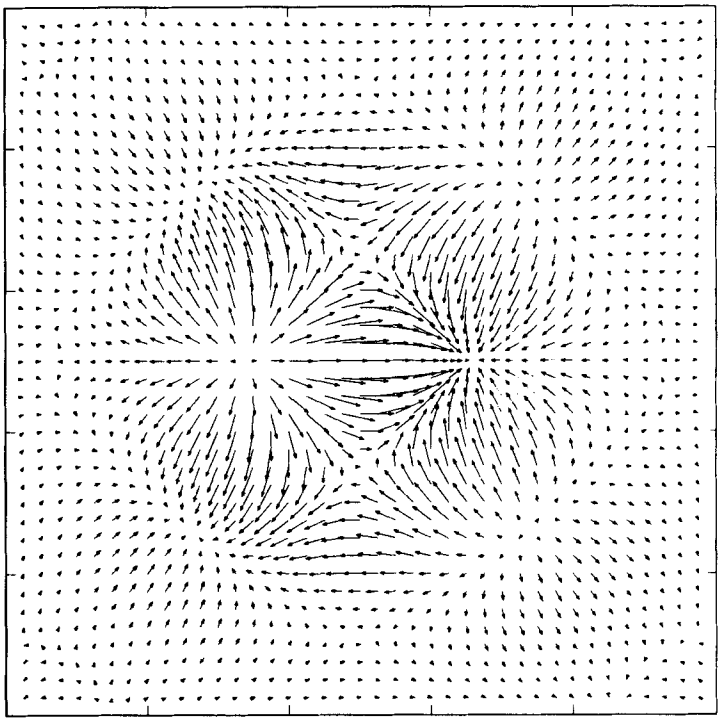

FIGURE 8. Horizontal velocity vectors at $z = 0.4$ for $\Gamma_x = \Gamma_y = 5$.

observed pattern ($N_c = 5$) exceeds $\mathscr{R}_c = 1800$ for our predicted pattern ($N_c = 4$) by only 2%.

Experimental values of $\mathscr{R}_c$ typically exceed our theoretical values. For example, Stork & Müller's $\mathscr{R}_c = 2400 \pm 40$ for $\Gamma = (2, 2)$ (their figure 4*a*) exceeds our corresponding value, 2106. Maurer & Libchaber (1979) obtained the experimental value $\mathscr{R}_c = 2300$ for three x-rolls and $\Gamma = (3.29, 1.88)$ compared to our $\mathscr{R}_c = 2013$. Differences may be due to partially conducting sidewalls in the experiments, since finite sidewall conductivity raises $\mathscr{R}_c$ (Catton 1972*b*; Charlson & Sani 1970).

In this complete description, the linear Oberbeck–Boussinesq equations require eigenfunctions with definite parity regardless of the aspect ratio. Figures 7(*c*) and 7(*d*) of Stork & Müller each exhibit a single narrow roll along one edge of a rectangular box, and therefore lack definite parity. Description of such flows probably requires a nonlinear analysis, which allows states of indefinite parity.

6. Conclusion

A correct treatment of onset of convection in boxes with small aspect ratios requires crossed rolls consisting of three-dimensional x-rolls and y-rolls. Three-dimensional effects are especially important for square or near-square boxes.

Experiments in boxes whose longest ratio of width to depth is near an odd number might further confirm our theoretical picture. Measurements of the growth-rate derivative for boxes would also be useful.

Helpful discussions with A. L. Fetter, R. P. Behringer, and Y. Maeno are gratefully acknowledged. Facilities at Stanford University, Sandia National Laboratories, and the Pittsburgh Supercomputing Center were useful in this work. This work was supported in part by U.S. National Science Foundation Grant No. DMR 81–18386 and the Office of Basic Energy Sciences, U.S. Department of Energy.

REFERENCES

BEHRINGER, R. P. & AHLERS, G. 1977 Heat transport and critical slowing down near the Rayleigh–Bénard instability in cylindrical containers. *Phys. Lett.* **62A**, 329.

CATTON, I. 1972*a* The effect of insulating vertical walls on the onset of motion in a fluid heated from below. *Intl J. Heat Mass Transfer* **15**, 665.

CATTON, I. 1972*b* Effect of wall conduction on the stability of a fluid in a rectangular region heated from below. *J. Heat Transfer* **94C**, 446.

CHANDRASEKHAR, S. 1961 *Hydrodynamic and Hydromagnetic Stability*. Clarendon.

CHARLSON, G. S. & SANI, R. L. 1970 Thermoconvective instability in a bounded cylindrical fluid layer. *Intl J. Heat Mass Transfer* **13**, 1479.

CHARLSON, G. S. & SANI, R. L. 1975 Finite amplitude axisymmetric thermoconvective flows in a bounded cylindrical layer of fluid. *J. Fluid Mech.* **71**, 209.

CLEVER, R. M. & BUSSE, F. H. 1974 Transition to time-dependent convection. *J. Fluid Mech.* **65**, 625.

CROSS, M. C. 1980 Derivation of the amplitude equation at the Rayleigh–Bénard instability. *Phys. Fluids* **23**, 1727.

DALLMANN, U. 1985 Structural stability of three-dimensional vortex flows. In *Nonlinear Dynamics of Transcritical Flows*. Lecture Notes in Engineering, vol. 13, p. 81. Springer.

DAVIES-JONES, R. P. 1970 Thermal convection in an infinite channel with no-slip sidewalls. *J. Fluid Mech.* **44**, 695.

DAVIS, S. H. 1967 Convection in a box: linear theory. *J. Fluid Mech.* **30**, 465.

EDWARDS, B. F. & FETTER, A. L. 1984 Onset of oscillations in Rayleigh–Bénard convection: horizontally unbounded slab. *Phys. Fluids* **27**, 2795.

HARRIS, D. L. & REID, W. H. 1958 On orthogonal functions which satisfy four boundary conditions. I. Tables for use with Fourier-type expansions. *Astrophys. J. Supp. Ser.* **33**, 429.

KOSCHMIEDER, E. L. 1966 On convection on a uniformly heated plane. *Beitr. Z. Phys. Atmos.* **39**, 1.

LUIJKX, J. M. & PLATTEN, J. K. 1981 On the onset of free convection in a rectangular channel. *J. Non-Equilibr. Therm.* **6**, 141.

MAENO, Y., HAUCKE, H. & WHEATLEY, J. 1985 Transition to oscillatory convection in a ^{3}He–Superfluid–^{4}He mixture. *Phys Rev. Lett.* **54**, 340.

MAURER, J. & LIBCHABER, A. 1979 Rayleigh–Bénard experiment in liquid helium; frequency locking and the onset of turbulence. *J. Phys. Lett. Paris* **40**, L-419.

REID, W. H. & HARRIS, D. L. 1958 On orthogonal functions which satisfy four boundary conditions. II. Integrals for use with Fourier-Type expansions. *Astrophys. J. Supp. Ser.* **33**, 448.

SHAUMEYER, J. N., BEHRINGER, R. P. & BAIERLEIN, R. 1981 Linear growth rates for the Rayleigh–Bénard instability in a cylindrical geometry. *J. Fluid Mech.* **109**, 339.

SCHLÜTER, A., LORTZ, D. & BUSSE, F. 1965 On the stability of steady finite amplitude convection. *J. Fluid Mech.* **23**, 129.

STEWARTSON, K. & WEINSTEIN, M. 1979 Marginal convection in a large rigid box. *Phys. Fluids* **22**, 1421.

STORK, K. & MÜLLER, U. 1972 Convection in boxes: experiments. *J. Fluid Mech.* **54**, 599.